DESY–08–129
23 September 2008

arXiv:0811.0894v1 [hep-ex] 6 Nov 2008

Measurement of beauty production from dimuon events at HERA

ZEUS Collaboration

Abstract

Beauty production in events containing two muons in the final state has been measured with the ZEUS detector at HERA using an integrated luminosity of 114 pb^{-1}. A low transverse-momentum threshold for muon identification, in combination with the large rapidity coverage of the ZEUS muon system, gives access to almost the full phase space for beauty production. The total cross section for beauty production in ep collisions at $\sqrt{s} = 318$ GeV has been measured to be $\sigma_{\rm tot}(ep \to b\bar{b}X) = 13.9 \pm 1.5({\rm stat.})^{+4.0}_{-4.3}({\rm syst.})$ nb. Differential cross sections and a measurement of $b\bar{b}$ correlations are also obtained, and compared to other beauty cross-section measurements, Monte Carlo models and next-to-leading-order QCD predictions.

The ZEUS Collaboration

S. Chekanov, M. Derrick, S. Magill, B. Musgrave, D. Nicholass[1], J. Repond, R. Yoshida
Argonne National Laboratory, Argonne, Illinois 60439-4815, USA [n]

M.C.K. Mattingly
Andrews University, Berrien Springs, Michigan 49104-0380, USA

P. Antonioli, G. Bari, L. Bellagamba, D. Boscherini, A. Bruni, G. Bruni, F. Cindolo, M. Corradi, G. Iacobucci, A. Margotti, R. Nania, A. Polini
INFN Bologna, Bologna, Italy [e]

S. Antonelli, M. Basile, M. Bindi, L. Cifarelli, A. Contin, S. De Pasquale[2], G. Sartorelli, A. Zichichi
University and INFN Bologna, Bologna, Italy [e]

D. Bartsch, I. Brock, H. Hartmann, E. Hilger, H.-P. Jakob, M. Jüngst, A.E. Nuncio-Quiroz, E. Paul, U. Samson, V. Schönberg, R. Shehzadi, M. Wlasenko
Physikalisches Institut der Universität Bonn, Bonn, Germany [b]

N.H. Brook, G.P. Heath, J.D. Morris
H.H. Wills Physics Laboratory, University of Bristol, Bristol, United Kingdom [m]

M. Kaur, P. Kaur[3], I. Singh[3]
Panjab University, Department of Physics, Chandigarh, India

M. Capua, S. Fazio, A. Mastroberardino, M. Schioppa, G. Susinno, E. Tassi
Calabria University, Physics Department and INFN, Cosenza, Italy [e]

J.Y. Kim
Chonnam National University, Kwangju, South Korea

Z.A. Ibrahim, B. Kamaluddin, W.A.T. Wan Abdullah
Jabatan Fizik, Universiti Malaya, 50603 Kuala Lumpur, Malaysia [r]

Y. Ning, Z. Ren, F. Sciulli
Nevis Laboratories, Columbia University, Irvington on Hudson, New York 10027 [o]

J. Chwastowski, A. Eskreys, J. Figiel, A. Galas, K. Olkiewicz, P. Stopa, L. Zawiejski
The Henryk Niewodniczanski Institute of Nuclear Physics, Polish Academy of Sciences, Cracow, Poland [i]

L. Adamczyk, T. Bołd, I. Grabowska-Bołd, D. Kisielewska, J. Łukasik, M. Przybycień, L. Suszycki
Faculty of Physics and Applied Computer Science, AGH-University of Science and Technology, Cracow, Poland [p]

A. Kotański[4], W. Słomiński[5]
Department of Physics, Jagellonian University, Cracow, Poland

O. Behnke, U. Behrens, I. Bloch[6], C. Blohm, A. Bonato, K. Borras, D. Bot, R. Ciesielski, N. Coppola, S. Fang, J. Fourletova[7], A. Geiser, P. Göttlicher[8], J. Grebenyuk, I. Gregor, O. Gutsche[6], T. Haas, W. Hain, A. Hüttmann, F. Januschek, B. Kahle, I.I. Katkov[9], U. Klein[10], U. Kötz, H. Kowalski, M. Lisovyi, E. Lobodzinska, B. Löhr, R. Mankel, I.-A. Melzer-Pellmann, S. Miglioranzi, A. Montanari, T. Namsoo, D. Notz[11], A. Parenti, L. Rinaldi[12], P. Roloff, I. Rubinsky, U. Schneekloth, A. Spiridonov[13], D. Szuba[14], J. Szuba[15], T. Theedt, J. Ukleja[16], G. Wolf, K. Wrona, A.G. Yagües Molina, C. Youngman, W. Zeuner[11]
Deutsches Elektronen-Synchrotron DESY, Hamburg, Germany

V. Drugakov, W. Lohmann, S. Schlenstedt
Deutsches Elektronen-Synchrotron DESY, Zeuthen, Germany

G. Barbagli, E. Gallo
INFN Florence, Florence, Italy [e]

P. G. Pelfer
University and INFN Florence, Florence, Italy [e]

A. Bamberger, D. Dobur, F. Karstens, N.N. Vlasov[17]
Fakultät für Physik der Universität Freiburg i.Br., Freiburg i.Br., Germany [b]

P.J. Bussey[18], A.T. Doyle, W. Dunne, M. Forrest, M. Rosin, D.H. Saxon, I.O. Skillicorn
Department of Physics and Astronomy, University of Glasgow, Glasgow, United Kingdom [m]

I. Gialas[19], K. Papageorgiu
Department of Engineering in Management and Finance, Univ. of Aegean, Greece

U. Holm, R. Klanner, E. Lohrmann, H. Perrey, P. Schleper, T. Schörner-Sadenius, J. Sztuk, H. Stadie, M. Turcato
Hamburg University, Institute of Exp. Physics, Hamburg, Germany [b]

C. Foudas, C. Fry, K.R. Long, A.D. Tapper
Imperial College London, High Energy Nuclear Physics Group, London, United Kingdom [m]

T. Matsumoto, K. Nagano, K. Tokushuku[20], S. Yamada, Y. Yamazaki[21]
Institute of Particle and Nuclear Studies, KEK, Tsukuba, Japan [f]

A.N. Barakbaev, E.G. Boos, N.S. Pokrovskiy, B.O. Zhautykov
Institute of Physics and Technology of Ministry of Education and Science of Kazakhstan, Almaty, Kazakhstan

V. Aushev[22], O. Bachynska, M. Borodin, I. Kadenko, A. Kozulia, V. Libov, D. Lontkovskyi, I. Makarenko, Iu. Sorokin, A. Verbytskyi, O. Volynets
Institute for Nuclear Research, National Academy of Sciences, Kiev and Kiev National University, Kiev, Ukraine

D. Son
Kyungpook National University, Center for High Energy Physics, Daegu, South Korea [g]

J. de Favereau, K. Piotrzkowski
Institut de Physique Nucléaire, Université Catholique de Louvain, Louvain-la-Neuve, Belgium [q]

F. Barreiro, C. Glasman, M. Jimenez, L. Labarga, J. del Peso, E. Ron, M. Soares, J. Terrón, M. Zambrana
Departamento de Física Teórica, Universidad Autónoma de Madrid, Madrid, Spain [l]

F. Corriveau, C. Liu, J. Schwartz, R. Walsh, C. Zhou
Department of Physics, McGill University, Montréal, Québec, Canada H3A 2T8 [a]

T. Tsurugai
Meiji Gakuin University, Faculty of General Education, Yokohama, Japan [f]

A. Antonov, B.A. Dolgoshein, D. Gladkov, V. Sosnovtsev, A. Stifutkin, S. Suchkov
Moscow Engineering Physics Institute, Moscow, Russia [j]

R.K. Dementiev, P.F. Ermolov †, L.K. Gladilin, Yu.A. Golubkov, L.A. Khein, I.A. Korzhavina, V.A. Kuzmin, B.B. Levchenko[23], O.Yu. Lukina, A.S. Proskuryakov, L.M. Shcheglova, D.S. Zotkin
Moscow State University, Institute of Nuclear Physics, Moscow, Russia [k]

I. Abt, A. Caldwell, D. Kollar, B. Reisert, W.B. Schmidke
Max-Planck-Institut für Physik, München, Germany

G. Grigorescu, A. Keramidas, E. Koffeman, P. Kooijman, A. Pellegrino, H. Tiecke, M. Vázquez[11], L. Wiggers
NIKHEF and University of Amsterdam, Amsterdam, Netherlands [h]

N. Brümmer, B. Bylsma, L.S. Durkin, A. Lee, T.Y. Ling
Physics Department, Ohio State University, Columbus, Ohio 43210 [n]

P.D. Allfrey, M.A. Bell, A.M. Cooper-Sarkar, R.C.E. Devenish, J. Ferrando, B. Foster, C. Gwenlan[24], K. Korcsak-Gorzo, K. Oliver, A. Robertson, C. Uribe-Estrada, R. Walczak
Department of Physics, University of Oxford, Oxford United Kingdom [m]

A. Bertolin, F. Dal Corso, S. Dusini, A. Longhin, L. Stanco
INFN Padova, Padova, Italy [e]

P. Bellan, R. Brugnera, R. Carlin, A. Garfagnini, S. Limentani
Dipartimento di Fisica dell' Università and INFN, Padova, Italy [e]

B.Y. Oh, A. Raval, J.J. Whitmore[25]
Department of Physics, Pennsylvania State University, University Park, Pennsylvania 16802 [o]

Y. Iga
Polytechnic University, Sagamihara, Japan [f]

G. D'Agostini, G. Marini, A. Nigro
Dipartimento di Fisica, Università 'La Sapienza' and INFN, Rome, Italy [e]

J.E. Cole[26], J.C. Hart
Rutherford Appleton Laboratory, Chilton, Didcot, Oxon, United Kingdom [m]

H. Abramowicz[27], R. Ingbir, S. Kananov, A. Levy, A. Stern
Raymond and Beverly Sackler Faculty of Exact Sciences, School of Physics, Tel Aviv University, Tel Aviv, Israel [d]

M. Kuze, J. Maeda
Department of Physics, Tokyo Institute of Technology, Tokyo, Japan [f]

R. Hori, S. Kagawa[28], N. Okazaki, S. Shimizu, T. Tawara
Department of Physics, University of Tokyo, Tokyo, Japan [f]

R. Hamatsu, H. Kaji[29], S. Kitamura[30], O. Ota[31], Y.D. Ri
Tokyo Metropolitan University, Department of Physics, Tokyo, Japan [f]

M. Costa, M.I. Ferrero, V. Monaco, R. Sacchi, A. Solano
Università di Torino and INFN, Torino, Italy [e]

M. Arneodo, M. Ruspa
Università del Piemonte Orientale, Novara, and INFN, Torino, Italy [e]

S. Fourletov[7], J.F. Martin, T.P. Stewart
Department of Physics, University of Toronto, Toronto, Ontario, Canada M5S 1A7 [a]

S.K. Boutle[19], J.M. Butterworth, T.W. Jones, J.H. Loizides, M. Wing[32]
Physics and Astronomy Department, University College London, London, United Kingdom [m]

B. Brzozowska, J. Ciborowski[33], G. Grzelak, P. Kulinski, P. Łużniak[34], J. Malka[34], R.J. Nowak, J.M. Pawlak, W. Perlanski[34], T. Tymieniecka, A.F. Żarnecki
Warsaw University, Institute of Experimental Physics, Warsaw, Poland

M. Adamus, P. Plucinski[35], A. Ukleja
Institute for Nuclear Studies, Warsaw, Poland

Y. Eisenberg, D. Hochman, U. Karshon
Department of Particle Physics, Weizmann Institute, Rehovot, Israel [c]

E. Brownson, D.D. Reeder, A.A. Savin, W.H. Smith, H. Wolfe
Department of Physics, University of Wisconsin, Madison, Wisconsin 53706, USA [n]

S. Bhadra, C.D. Catterall, Y. Cui, G. Hartner, S. Menary, U. Noor, J. Standage, J. Whyte
Department of Physics, York University, Ontario, Canada M3J 1P3 [a]

[1] also affiliated with University College London, United Kingdom
[2] now at University of Salerno, Italy
[3] also working at Max Planck Institute, Munich, Germany
[4] supported by the research grant no. 1 P03B 04529 (2005-2008)
[5] This work was supported in part by the Marie Curie Actions Transfer of Knowledge project COCOS (contract MTKD-CT-2004-517186)
[6] now at Fermilab, Batavia, Illinois, USA
[7] now at University of Bonn, Germany
[8] now at DESY group FEB, Hamburg, Germany
[9] also at Moscow State University, Russia
[10] now at University of Liverpool, UK
[11] now at CERN, Geneva, Switzerland
[12] now at Bologna University, Bologna, Italy
[13] also at Institut of Theoretical and Experimental Physics, Moscow, Russia
[14] also at INP, Cracow, Poland
[15] also at FPACS, AGH-UST, Cracow, Poland
[16] partially supported by Warsaw University, Poland
[17] partly supported by Moscow State University, Russia
[18] Royal Society of Edinburgh, Scottish Executive Support Research Fellow
[19] also affiliated with DESY, Germany
[20] also at University of Tokyo, Japan
[21] now at Kobe University, Japan
[22] supported by DESY, Germany
[23] partly supported by Russian Foundation for Basic Research grant no. 05-02-39028-NSFC-a
[24] STFC Advanced Fellow
[25] This material was based on work supported by the National Science Foundation, while working at the Foundation.
[26] now at University of Kansas, Lawrence, USA
[27] also at Max Planck Institute, Munich, Germany, Alexander von Humboldt Research Award
[28] now at KEK, Tsukuba, Japan
[29] now at Nagoya University, Japan
[30] member of Department of Radiological Science, Tokyo Metropolitan University, Japan
[31] now at SunMelx Co. Ltd., Tokyo, Japan
[32] also at Hamburg University, Inst. of Exp. Physics, Alexander von Humboldt Research Award and partially supported by DESY, Hamburg, Germany
[33] also at Łódź University, Poland
[34] member of Łódź University, Poland
[35] now at Lund Universtiy, Lund, Sweden
† deceased

[a] supported by the Natural Sciences and Engineering Research Council of Canada (NSERC)

[b] supported by the German Federal Ministry for Education and Research (BMBF), under contract numbers 05 HZ6PDA, 05 HZ6GUA, 05 HZ6VFA and 05 HZ4KHA

[c] supported in part by the MINERVA Gesellschaft für Forschung GmbH, the Israel Science Foundation (grant no. 293/02-11.2) and the U.S.-Israel Binational Science Foundation

[d] supported by the Israel Science Foundation

[e] supported by the Italian National Institute for Nuclear Physics (INFN)

[f] supported by the Japanese Ministry of Education, Culture, Sports, Science and Technology (MEXT) and its grants for Scientific Research

[g] supported by the Korean Ministry of Education and Korea Science and Engineering Foundation

[h] supported by the Netherlands Foundation for Research on Matter (FOM)

[i] supported by the Polish State Committee for Scientific Research, project no. DESY/256/2006 - 154/DES/2006/03

[j] partially supported by the German Federal Ministry for Education and Research (BMBF)

[k] supported by RF Presidential grant N 8122.2006.2 for the leading scientific schools and by the Russian Ministry of Education and Science through its grant for Scientific Research on High Energy Physics

[l] supported by the Spanish Ministry of Education and Science through funds provided by CICYT

[m] supported by the Science and Technology Facilities Council, UK

[n] supported by the US Department of Energy

[o] supported by the US National Science Foundation. Any opinion, findings and conclusions or recommendations expressed in this material are those of the authors and do not necessarily reflect the views of the National Science Foundation.

[p] supported by the Polish Ministry of Science and Higher Education as a scientific project (2006-2008)

[q] supported by FNRS and its associated funds (IISN and FRIA) and by an Inter-University Attraction Poles Programme subsidised by the Belgian Federal Science Policy Office

[r] supported by the Malaysian Ministry of Science, Technology and Innovation/Akademi Sains Malaysia grant SAGA 66-02-03-0048

1 Introduction

The production of beauty quarks in ep collisions at HERA provides a stringent test of perturbative Quantum Chromodynamics (QCD), since the large b-quark mass ($m_b \sim 5\,\mathrm{GeV}$) gives a hard scale that should ensure reliable predictions in all regions of phase space, including the kinematic threshold. Especially in this region, with b-quark transverse momenta comparable to or less than the b-quark mass, next-to-leading-order (NLO) QCD calculations in which the (massive) b quarks are generated dynamically are expected to provide accurate predictions [1, 2].

The cross section for beauty production has been measured in $p\bar{p}$ collisions at the S$p\bar{p}$S [3] and Tevatron colliders [4], in $\gamma\gamma$ interactions at LEP [5, 6], and in fixed-target πN [7] and pN [8] experiments. Most results, including recent results from the Tevatron, are in good agreement with QCD predictions. Large discrepancies are observed in some [5] of the results from $\gamma\gamma$ interactions at LEP.

In most of the previous measurements of beauty production at HERA, beauty events were selected by requiring the presence of one or more jets, tagged by a muon or electron from the semi-leptonic decay of one of the b quarks [9–13], or by tracks originating from the secondary decay vertex of beauty hadrons [14]. This restricts the measurements to b quarks with high transverse momentum (p_T).

This paper reports measurements of beauty production via the reaction $ep \to b\bar{b}X \to \mu\mu X'$ using the ZEUS detector at HERA. The dimuon final state yields a data sample enriched in $b\bar{b}$ pairs, and with strongly suppressed backgrounds from other processes. This allows low muon-p_T (p_T^μ) thresholds to be applied without any jet requirements, and gives access to a larger region of phase space, especially towards lower transverse momenta of the b quarks.

Conceptually, the analysis is similar to the H1 and ZEUS analyses of beauty in $D^*\mu$ final states [15, 16], with three significant differences. The larger branching ratio yields higher statistics, so that differential cross sections can be measured. The wider rapidity coverage and very low p_T threshold allow the extraction of the total beauty cross section with little extrapolation. The low charm background in the dimuon final state, partially due to the harder b fragmentation, allows measurements of $b\bar{b}$ correlations, testing the influence of higher-order contributions on the perturbative calculations.

2 Experimental set-up

The data sample used in this analysis corresponds to an integrated luminosity $\mathcal{L} = 114.1 \pm 2.3\ \mathrm{pb}^{-1}$, collected with the ZEUS detector from 1996 to 2000. In 1996–97,

HERA provided collisions between an electron[1] beam of $E_e = 27.5\,\text{GeV}$ and a proton beam of $E_p = 820\,\text{GeV}$, corresponding to a centre-of-mass energy $\sqrt{s} = 300\,\text{GeV}$ ($\mathcal{L}_{300} = 38.0 \pm 0.6\ \text{pb}^{-1}$). In 1998–2000, the proton-beam energy was $E_p = 920\,\text{GeV}$, corresponding to $\sqrt{s} = 318\,\text{GeV}$ ($\mathcal{L}_{318} = 76.1 \pm 1.7\ \text{pb}^{-1}$).

A detailed description of the ZEUS detector can be found elsewhere [17]. A brief outline of the components most relevant for this analysis is given below.

Charged particles were tracked in the central tracking detector (CTD) [18], which operated in a magnetic field of 1.43 T provided by a thin superconducting coil. The CTD consisted of 72 cylindrical drift chamber layers, organised in 9 superlayers covering the polar-angle[2] region $15^\circ < \theta < 164^\circ$. The transverse-momentum resolution for full-length tracks was $\sigma(p_T)/p_T = 0.0058 p_T \oplus 0.0065 \oplus 0.0014/p_T$, with p_T in GeV.

The high-resolution uranium-scintillator calorimeter (CAL) [19] consisted of three parts: the forward (FCAL), the barrel (BCAL) and the rear (RCAL) calorimeters. Each part was subdivided transversely into towers and longitudinally into one electromagnetic section (EMC) and either one (in RCAL) or two (in BCAL and FCAL) hadronic sections (HAC). The smallest subdivision of the calorimeter is called a cell. The CAL energy resolutions, as measured under test-beam conditions, were $\sigma(E)/E = 0.18/\sqrt{E}$ for electrons and $\sigma(E)/E = 0.35/\sqrt{E}$ for hadrons, with E in GeV.

The muon system consisted of rear, barrel (R/BMUON) [20] and forward (FMUON) [17] tracking detectors. The B/RMUON consisted of limited-streamer (LS) tube chambers placed behind the BCAL (RCAL), inside and outside the magnetised iron yoke surrounding the CAL. The barrel and rear muon chambers covered polar angles from 34° to 135° and from 135° to 171°, respectively. The FMUON consisted of six planes of LS tubes and four planes of drift chambers covering the angular region from 5° to 32°. The muon system exploited the magnetic field of the iron yoke and, in the forward direction, of two iron toroids magnetised to 1.6 T to provide an independent measurement of the muon momentum.

Muons were also detected by the sampling Backing Calorimeter (BAC) [21]. This detector consisted of 5200 proportional drift chambers which were typically 5 m long and had a wire spacing of 1 cm. The chambers were inserted into the iron yoke of the ZEUS detector (barrel and two end caps) covering the CAL. The BAC was equipped with analogue

[1] Electrons and positrons are both referred to as electrons in this paper.

[2] The ZEUS coordinate system is a right-handed Cartesian system, with the Z axis pointing in the proton beam direction, referred to as the "forward direction", and the X axis pointing left towards the centre of HERA. The coordinate origin is at the nominal interaction point. The pseudorapidity is defined as $\eta = -\ln\left(\tan\frac{\theta}{2}\right)$, where the polar angle, θ, is measured with respect to the proton beam direction.

readout for energy measurement and digital readout for muon tracking. The former was based on 2000 towers (50×50 cm^2), providing an energy resolution of $\sim 100\%/\sqrt{E}$. The digital information from the wires allowed the reconstruction of muon trajectories in two dimensions (XY in barrel and YZ in end caps) with an accuracy of a few mm.

3 Principle of the measurement

Events with at least two muons in the final state were selected. Two principal event classes contribute to the beauty signal to be measured. The first consists of events in which the two muons originate from the same parent b quark[3], e.g. through the sequential decay chain $b \to c\mu X \to s\mu\mu X'$. These yield unlike-sign muon pairs produced in the same event hemisphere and with dimuon invariant masses of $m_{\rm inv}^{\mu\mu} < 4$ GeV (i.e. a partially reconstructed B-meson mass). The second class consists of events in which the two muons originate from different beauty quarks of a $b\bar{b}$ pair. These can yield both like- and unlike-sign dimuon combinations, depending on whether the muon originates from the decay of the primary beauty quark, or from a secondary charm quark. In addition, $B^0\bar{B}^0$ mixing can dilute these charge correlations. Muons from different b quarks will predominantly be produced in different hemispheres, and tend to have a large dimuon mass.

An important background contribution arises from primary charm-quark pair production where both charm quarks decay into a muon. This yields unlike-sign muon pairs only, with the two muons produced predominantly in opposite hemispheres. Since this background is too small to be measured directly from the dimuon data, it was normalised to the charm contribution as determined from the ZEUS $D^* + \mu$ sample [16] which has a similar event topology and covers a similar though somewhat more restricted kinematic range.

Other backgrounds yielding unlike-sign muon pairs include heavy quarkonium decays and Bethe-Heitler (BH) processes. In contrast to muons from semileptonic decays, muons from these sources are not directly accompanied by hadronic activity, thus giving an isolated muon signature.

Beauty production is the only source of genuine like-sign muon pairs. Background contributions to both like- and unlike-sign combinations include events in which either one or both muons are false, i.e. originate from $K \to \mu$ or $\pi \to \mu$ decays in flight or are misidentified hadrons. Studies [22] have shown that the charges of such false-muon pairs are almost uncorrelated, i.e. the contributions to the like- and unlike-sign dimuon distributions are almost equal. The difference between the unlike- ($N_{\rm data}^{\rm u}$) and like-sign ($N_{\rm data}^{\rm l}$) distributions is thus essentially free from false-muon background, without the need to simulate

[3] Unless stated otherwise, throughout this paper, the term b quark includes $\bar{b}$.

this background using Monte Carlo (MC) methods. Once the background contributions from open charm ($N_{\rm charm}$), J/ψ and other heavy vector mesons ($N_{\rm VM}$) and Bethe-Heitler ($N_{\rm BH}$) are known, this difference can be used to measure the beauty contribution $N_{b\bar{b}\to\mu\mu}$ according to the formula

$$N_{b\bar{b}\to\mu\mu} = \left(N^{\rm u}_{\rm data} - N^{\rm l}_{\rm data} - (N_{\rm charm} + N_{\rm VM} + N_{\rm BH})\right) \times \left(\frac{N^{\rm u}_{b\bar{b}} + N^{\rm l}_{b\bar{b}}}{N^{\rm u}_{b\bar{b}} - N^{\rm l}_{b\bar{b}}}\right)^{\rm MC} \qquad (1)$$

where the last term refers to the unlike-sign ($N^{\rm u}_{b\bar{b}}$) and like-sign ($N^{\rm l}_{b\bar{b}}$) beauty contributions predicted by the MC. Small corrections to this procedure will be explained in Section 7. The beauty signal is hence extracted from the difference between the unlike- and like-sign samples.

The like-sign false-muon background can then be obtained from the data by subtracting the MC like-sign beauty contribution, properly scaled to the measurement, from the total like-sign sample, while the unlike-sign background is a simple reflection of the like-sign background. This method to obtain the false-muon background contributions will be referred to as the subtraction method.

Since one of the goals is the determination of the total beauty production cross section in ep collisions, events from deep inelastic scattering (DIS), where the photon virtuality, Q^2, is larger than $1\,\mathrm{GeV}^2$, and photoproduction ($Q^2 < 1$ GeV^2) were not explicitly separated.

The average cross sections obtained from the two different running periods ($\sqrt{s} = 300$ and 318 GeV) are all expressed in terms of a single cross section at $\sqrt{s} = 318$ GeV. This involves a typical correction of +2%.

4 Event selection and reconstruction

4.1 Trigger selection

The data were selected online by means of a three-level trigger system [17, 23] through an inclusive "or" of four different trigger channels:

- a muon reaching the inner B/RMUON chambers and matched to a minimum ionising energy deposit (MIP) in the CAL or any muon reaching the outer B/RMUON chambers (muon channel);
- a reconstructed D meson candidate (D^* channel [24], plus similar chains for other charm mesons [25]);
- two jets (dijet channel [11]);

- a scattered-electron candidate in the CAL (DIS channel [12]).

For part of the data taking, the requirements on the DIS and dijet channels were loosened in the presence of any muon in the inner B/RMUON chambers. The non-muon triggers were used to gain geometric acceptance for regions not covered by the B/RMUON chambers, and to evaluate the efficiency of the muon triggers. Owing to this redundancy, the trigger efficiency for dimuon events with reconstructed muons from beauty was high, $80 \pm 4\%$.

4.2 Event selection

The large mass of a $b\bar{b}$ pair, at least ~ 10 GeV, usually leads to a significant amount of energy deposited in the more central parts of the detector. To suppress backgrounds from false-muon events and charm, a hadronic transverse energy cut

$$E_T \geq 8 \text{ GeV}$$

was applied, where

$$E_T = \begin{cases} E_T^{\theta>10^\circ} & \text{no scattered electron} \\ E_T^{\theta>10^\circ} - E_T^e & \text{with scattered electron.} \end{cases}$$

The transverse energy was calculated as $E_T^{\theta>10^\circ} = \Sigma_{i,\theta_i>10^\circ}(E_i \sin\theta_i)$, where the sum runs over all energy deposits in the CAL with the polar angle above 10°. The latter restriction is imposed to remove proton-remnant effects. If detected, the energy of the scattered electron (E_T^e) was subtracted. The detection criteria for the scattered electron were the same as in a previous publication [16].

Various tracking requirements were imposed [22], the most important of which was that the reconstructed longitudinal vertex position should be consistent with an ep interaction, $|Z_{\text{vtx}}| < 50$ cm.

4.3 Muon selection

Muons were reconstructed offline using an inclusive "or" of the following procedures:

- a muon track was found in the inner B/RMUON chambers. A match in position and angle to a CTD track was required. In the bottom region, where no inner chambers are present, the outer chambers were used instead. If a match was found to both inner and outer chambers, a momentum-matching criterion was added;

- a muon track was found in the FMUON chambers. Within the CTD acceptance, a match in position and angle to a CTD track was required and the momentum was obtained from a combined fit of the CTD and FMUON information. Outside the CTD acceptance, candidates well measured in FMUON only and fitted to the primary vertex were accepted;
- a muon track or localised energy deposit was found in the BAC, and matched to a CTD track, from which the muon momentum was obtained. In the forward region of the detector, a MIP in the calorimeter was required in addition in order to reduce background related to the proton beam or to the punch-through of high energy hadrons.

Most muons are within the geometric acceptance of more than one of these algorithms. The overall efficiency is about 80% for high-momentum muons (more than 2-5 GeV, depending on η).

Two different kinematic selections were made. In the barrel region, the requirement that the muons reach at least the inner muon chambers implies a muon transverse momentum (p_T^μ) of about 1.5 GeV or more. In order to have uniform kinematic acceptance, a cut

$$p_T^\mu > 1.5\,\mathrm{GeV}$$

was therefore applied to all muons (selection A).

In the forward and rear regions, lower p_T muons can be detected, although with somewhat higher background. To cover the largest possible phase space for the intended measurement of a total beauty-production cross section, the p_T cut was lowered to

$$p_T^\mu > 0.75\,\mathrm{GeV}$$

for high-quality muons [22], i.e. muons seen by more than one muon detector and/or confirmed by a MIP in the CAL (selection B). For other muons satisfying all previously listed criteria, the cut $p_T^\mu > 1.5\,\mathrm{GeV}$ was retained to keep the background low. Selection A is thus a subset of selection B.

At least two such muon candidates were required per event. No explicit cut on the muon angle was applied for either selection. The angular coverage of the muon chambers, BAC and CTD gives continuous useable acceptance in the pseudorapidity region

$$-2.2 \lesssim \eta^\mu \lesssim 2.5\ .$$

To suppress events with ambiguous matches between CTD tracks and muon chamber segments as well as genuine dimuons from prompt light-meson decays (e.g. $\rho \to \mu\mu$), a dimuon invariant mass ($m^{\mu\mu}$) cut of

$$m^{\mu\mu} > 1.5\ \ \mathrm{GeV}$$

was applied. This implies a minimum opening angle between the two muons.

Events with a very forward and a very backward muon candidate, a topology not favoured for the beauty signal, were removed by a cut on the difference in pseudorapidity of the two muon candidates of

$$|\eta^{\mu_1} - \eta^{\mu_2}| < 3.0.$$

Muon candidates with badly measured momentum (predominantly from false-muon backgrounds) were suppressed using the imbalance between the transverse momenta of the muons

$$(|p_T^{\mu_1} - p_T^{\mu_2}|)/(p_T^{\mu_1} + p_T^{\mu_2}) < 0.7.$$

An additional cut with a similar scope as the initial E_T cut was applied on the fraction of the total transverse energy carried by the muon pair

$$0.1 < (p_T^{\mu_1} + p_T^{\mu_2})/E_T < \begin{cases} 0.5 & \text{for } m^{\mu\mu} < 4 \text{ GeV} \\ 0.7 & \text{for } m^{\mu\mu} \geq 4 \text{ GeV}. \end{cases}$$

The reason for the distinction of the two different dimuon mass regions will be explained in Section 7. This E_T-fraction cut removes events where the hadronic activity is, respectively, very high (false-muon background) or low (quarkonia and Bethe-Heitler).

Cosmic-ray muons were removed by discarding events with back-to-back muon candidates and events in which the average calorimeter timing differs by more than 10 ns from the nominal collision time. Large cosmic showers were removed using the BAC total energy and number of BAC muon segments.

A sample of 4146 dimuon events was obtained using selection B. Selection A retained about two thirds of these events.

4.4 Muon isolation

Muons from semileptonic decays are usually not isolated, i.e. they are normally accompanied by hadrons originating from the fragmentation and decay of the parent heavy quark and from other hadronic activity in the event. Hadronic activity in the detector was reconstructed using a combination of both track and calorimeter information [26] referred to as energy-flow objects (EFOs). The difference in azimuth angle and pseudorapity, $\Delta\phi$ and $\Delta\eta$, was calculated between each EFO and each muon candidate in the event. The total transverse energy, $I_{1,2}$, deposited in a cone of $\Delta R = \sqrt{\Delta\phi^2 + \Delta\eta^2} < 1$ around each muon flight direction was calculated by summing over all relevant EFOs, excluding the other muon. Since usually either both (beauty signal and open charm) or neither (elastic J/ψ, Bethe-Heitler, etc.) of the muons arise from semileptonic decays, the quadratic

sum $I^{\mu\mu} = \sqrt{I_1^2 + I_2^2}$ of the two energy sums was found to yield the best sensitivity to distinguish between the two cases.

5 Background and event simulation

In order to measure the beauty signal, several background contributions to the selected data sample were evaluated:

- the background from open charm decays not originating from beauty;
- the background from quarkonium states not originating from open beauty (J/ψ, ψ', Υ, ...), produced in elastic or inelastic collisions;
- the background from Bethe-Heitler muon pair production;
- the background from false muons.

Monte Carlo simulations of beauty and charm production were performed using the generators PYTHIA [27] (for events with $Q^2 < 1$ GeV^2) and RAPGAP [28] (for $Q^2 > 1$ GeV^2). These simulations include the direct photon-gluon fusion process ($\gamma g \to Q\bar{Q}$, $Q = b, c$), flavour excitation in the resolved photon and proton (e.g. $Qg \to Qg$, $\gamma Q \to Qg$), and hadron-like resolved photon processes (e.g. $gg \to Q\bar{Q}$). Gluon splitting into heavy flavours ($g \to Q\bar{Q}$) in the initial or final states of light-quark events was not included in the simulations; this contribution is, however, expected to be small [29].

Inelastic quarkonium production was simulated using HERWIG [30], while elastic quarkonia and Bethe-Heitler processes were produced using several generators including GRAPE [31].

The ZEUS detector response, including the transformation of MC truth level quantities into reconstructed quantities, was simulated in detail using a programme based on GEANT 3.13 [32]. The detector simulation for beauty and charm events includes the simulation of both real and false muons.

Fake muons can be produced by hadron showers leaking from the back of the calorimeter or by charged hadrons traversing the entire calorimeter without interaction. In addition, low-momentum muons can originate from in-flight decays of pions and kaons. Tracks reconstructed in the central tracker may also be erroneously associated to a signal from a real muon in the muon chambers. A study [29] based on pions from K^0 decays, protons from Λ decays, and kaons from ϕ and D^* decays, showed that the detector simulation reproduced these backgrounds reasonably well. They will be collectively referred to as false muons.

Backgrounds from false muons in events not containing charm or beauty were not simulated. They were estimated from the data using the subtraction method described in Section 3.

Since the muon range in dense material (effective momentum threshold) and the muon detector efficiencies were imperfectly simulated, corrections to the MC were determined [22] using an independent data set consisting of isolated J/ψ and Bethe-Heitler events. Tabulated as a function of p_T^μ and η^μ, these corrections were applied to MC events on an event-by-event basis.

6 Theoretical predictions and uncertainties

The MC programs described earlier, based on leading-order (LO) matrix elements with the addition of parton showers (PS) to obtain higher-order topologies, were used for the acceptance corrections. These programs are expected to describe the shapes of differential distributions, but not necessarily their normalisation. For quantitative comparisons with QCD, next-to-leading-order (NLO) predictions are used.

QCD calculations in which b quarks are treated as massless particles [33] are not applicable in the kinematic range relevant here. Calculations based on CCFM parton-evolution schemes [34], also called k_T factorisation, do not yet exist with full NLO implementation. Fixed-order NLO calculations with massive b quarks were therefore chosen as the reference predictions.

The NLO FMNR program [1] evaluates parton-level cross sections for beauty in γp collisions (photoproduction) in the fixed-order massive mode, for both pointlike and hadron-like photon couplings to the heavy quarks. The Weizsäcker-Williams (WW) approximation with an effective $Q^2_{\rm max}$ cutoff of 25 GeV^2 ($\sim m_b^2$) [35] was used to evaluate and include the DIS contribution to the cross sections, which is approximately 15%. This is in agreement with the DIS prediction from HVQDIS described below.

The parton-density functions used were CTEQ5M [36] for the proton, and GRV-G-HO [37] for the photon. The renormalisation and factorisation scales μ were chosen to be equal and parametrised by $\mu_0 = \sqrt{p_T^2 + m_b^2}/2$, where p_T is the average transverse momentum of the two emerging b quarks, and $m_b = 4.75$ GeV is the b-quark mass. Such a scale choice is equivalent to the choice $\mu_0 = E_T/2$ or $\mu_0 = \sqrt{E_T^2 + Q^2}/2$ used in many jet measurements at the Tevatron [38] and at HERA [39], and is expected to compensate somewhat for uncalculated higher-order contributions [40]. An estimate of the theoretical uncertainty was obtained by simultaneously varying $4.5 < m_b < 5.0$ GeV and $\mu_0/2 < \mu < 2\mu_0$ such that the uncertainty was maximised. Typical uncertainties resulting from this procedure (e.g. for the $b\bar{b}$ total cross section) are $+60\%$ and -30%. Variations of the parton densities

and the strong coupling parameter, $\Lambda_{\rm QCD}$, led to uncertainties which were much smaller than the uncertainties related to mass and scale variations. They were therefore neglected.

Predictions for visible $\mu\mu$ final states were obtained by linking the FMNR parton-level predictions to the fragmentation and decay chain provided by PYTHIA using the FMNR⊗PYTHIA interface [41]. Additional parton showering was not applied[4]. The branching ratios were corrected to correspond to those obtained from the Particle Data Group (PDG) [43], as listed in Table 1. All other parameters, including those for fragmentation, and the procedure to obtain their uncertainties, were the same as in an earlier analysis [16], and described elsewhere [41].

The DIS part of the inclusive cross section is also calculated using the NLO predictions from HVQDIS [2]. Only point-like contributions are included in this prediction. The parton density function used was CTEQ5F4 [36]. The renormalisation and factorisation scales μ were chosen to be equal and parametrised by $\mu_0 = \sqrt{p_T^2 + m_b^2 + Q^2}/2$. The mass and scales were varied as for FMNR. A scheme for the calculation of visible cross sections for correlated final states, corresponding to the FMNR⊗PYTHIA interface described above, was not available. Therefore, DIS cross-section comparisons are limited to parton level, and the DIS contribution to the inclusive cross sections is included in the FMNR⊗PYTHIA predictions via the WW approximation.

7 Signal extraction

Dimuon mass and charge separation

As motivated in Section 3, events were separated by the muon charges into like- and unlike-sign dimuon samples. To differentiate between muon pairs from the cascade decay of *the same* b quark and those from *different* b quarks, the distributions were further separated depending on the dimuon invariant mass: low-mass dimuons with $m^{\mu\mu} < 4$ GeV, enriched in muons from the same b quark, and high-mass dimuons with $m^{\mu\mu} > 4$ GeV, containing dimuons originating from the decay of different b quarks only. The dominant signal and background contributions to the four subsamples are summarised in Table 2.

The resulting dimuon mass distributions for the low- and high-mass, like- and unlike-sign subsamples for selection B are shown in Fig. 1. The MC distributions were in each case normalised to the data according to the procedure described in the following subsections. The high-mass region is already strongly beauty enriched, while the low-mass region

[4] The MC@NLO approach [42], which allows the combination of NLO matrix elements with parton showers, is not yet available for *ep* interactions.

exhibits a significant contribution from J/ψ production not originating from B hadron[5] decays. Such dimuon pairs tend to be isolated.

Dimuon isolation cuts

To reduce this J/ψ contribution, as well as corresponding contributions from ψ', Υ and Bethe-Heitler processes, a non-isolation requirement was applied, based on the fact that muons from semileptonic decays are accompanied by hadrons from the same decay. The dimuon isolation variable $I^{\mu\mu}$, defined in Section 4.4, was required to exceed 250 MeV, safely above the noise level of the CAL. This reduces the elastic quarkonium and Bethe-Heitler contributions to an almost negligible level.

Inelastic quarkonium and Bethe-Heitler events might pass the above cut because hadrons from e.g. the proton remnant can accidentally end up in the isolation cone. For events in the J/ψ and ψ' mass peaks, where this background is largest, the cut was therefore raised to 2 GeV.

In summary, dimuons fulfilling the relation

$$I^{\mu\mu} \geq \begin{cases} 2.0 \text{ GeV} & \text{for } m^{\mu\mu} \in [2.9,\ 3.25] \text{ GeV or } m^{\mu\mu} \in [3.6,\ 3.75] \text{ GeV} \\ 0.25 \text{ GeV} & \text{otherwise} \end{cases}$$

are called non-isolated. This additional requirement is satisfied by 3500 events from selection B. The other events form a complementary isolated background sample.

Figure 2 shows the muon p_T and η distributions for non-isolated unlike-sign dimuon pairs, combining the low- and high-mass samples. The remaining contribution from J/ψ, Bethe-Heitler, etc. processes was normalised to the isolated background sample. The charm contribution is small and was normalised to the charm signal in the $D^* + \mu$ sample [16] as outlined in Section 3. The different contributions to Fig. 2 are listed in Table 3.

Signal evaluation

The beauty signal and false-muon background were obtained using the procedure described in Section 3. However, some further corrections are needed. Events from unlike-sign background sources, such as charm, which have been reconstructed as like-sign dimuon events due to false muons, are included both in the false-muon background estimation and in the MC samples. To avoid double counting, this (very small) contribution is subtracted from the MC samples. False muons in the beauty MC are considered as part of the signal.

[5] The term B hadron includes b baryons.

The signal extraction procedure according to Eq. (1) relies on the unlike- and like-sign false-muon background contributions being equal. A dedicated false-muon background study [22] revealed a small residual excess of unlike-sign over like-sign background. This excess was corrected for using a multiplicative correction factor, $\alpha_{\rm corr}$, of 1.02 for the high-mass and 1.06 for the low-mass dimuon sample. The beauty fraction was thus determined using a modified version of Eq. (1)

$$N_{b\bar{b}\to\mu\mu} = \left(N^{\rm u}_{\rm data} - \alpha_{\rm corr}\cdot N^{\rm l}_{\rm data} - (N_{\rm charm} + N_{\rm VM} + N_{\rm BH})\right) \times \left(\frac{N^{\rm u}_{b\bar{b}} + N^{\rm l}_{b\bar{b}}}{N^{\rm u}_{b\bar{b}} - \alpha_{\rm corr}\cdot N^{\rm l}_{b\bar{b}}}\right)^{\rm MC} . \quad (2)$$

A total of 1783 of the 3500 non-isolated events from selection B were found to originate from beauty, corresponding to a beauty fraction of 51%.

8 Systematic uncertainties

The main sources of systematic uncertainty for the measurement of visible cross sections are described in this section, in approximate order of importance. The numbers in parentheses refer to the specific case of the inclusive visible cross section of Section 9. Bin-by-bin uncertainties were evaluated for the differential distributions where possible and appropriate. They are mostly similar to those derived for the inclusive visible cross section. Additional uncertainties introduced by the extrapolation to quark-level cross sections are discussed in Section 9.

- **Muon efficiency correction.** The muon efficiency, including the efficiency of the muon chambers and of the MUON-CTD matching, is known to about 7% from a study based on an independent muon sample, and from the variance of the cross section when information from different muon detectors is used independently [22]. Conservatively, it is assumed to be fully correlated between the two muons ($\pm$15%).
- **Normalisation of charm background.** The transfer of the normalisation of the charm contribution from the $D^*\mu$ analysis [16] to this analysis involves the following uncertainties: the statistical error of the fit of the charm contribution, $\pm$10%; the inclusive branching ratio $c \to \mu$, $\pm$10%; the acceptance uncertainty due to charm fragmentation and decay spectra, $\pm$10%; the fragmentation fraction $c \to D^{*\pm}$, $\pm$6%; the branching ratio $D^{*\pm} \to K\pi\pi$, $\pm$3%; and the use of all muon detectors (this analysis) versus the use of the barrel and rear muon chambers only [16], $\pm$10%. The influence of the correlation between the fitted beauty and charm fractions in the $D^*\mu$ analysis [16] was found to be negligible. The normalisation of the charm contribution was varied by 21% according to the resulting combined uncertainty ($\pm$12%).

- **Normalisation of the Bethe-Heitler, J/ψ, etc. backgrounds.** The normalisation of the residual non-isolated contributions from Bethe-Heitler, charmonium, and Υ production was varied by $\pm 50\%$ ($\pm 10\%$).
- **False-muon background.** As a cross check for the determination of the false-muon background by the subtraction method, the probability of a reconstructed hadron to be misidentified as a muon was obtained from an inclusive dijet MC sample and tabulated as a function of p_T and η. Starting from a data sample with selection cuts identical to the present analysis, except that only one muon candidate was required, false-dimuon events were created by assuming a suitable additional hadron to be identified as a muon according to this tabulated probability. After corrections for trigger efficiency, and for the contribution from one false and one true muon obtained directly from the b and c MC, an independent background prediction was obtained [44]. It agreed very well in both normalisation and shape with that of the default subtraction method, thus confirming the method. Since the uncertainty on this background is already implicitly contained in the statistical error of the subtraction method, no explicit additional uncertainty was assigned.
- **b spectral shape uncertainty and $b\bar{b}$ correlations.** It was checked that the b-quark spectra from Pythia and Rapgap agree well with the corresponding spectra from the NLO predictions described below [29]. To estimate the effect of variations of this shape, and of effects of variations of the $b\bar{b}$ correlations for different topologies on the efficiency, the efficiency was evaluated using the Pythia direct contribution only, or doubling the non-direct contributions ($+4\%/-12\%$).
- **$B^0\bar{B}^0$ oscillations.** The $B^0\bar{B}^0$ oscillation parameter was varied by 8%. This includes the uncertainties of the mixing implementation in the MC models used ($\pm 4\%$).
- **Other b MC model uncertainties.** This includes the uncertainty of the procedure used to account for differences of the branching ratios in the signal MC and Table 1, the uncertainty from b fragmentation, and from the shape of the lepton spectrum from b decays ($\pm$ 10%).
- **c spectral shape uncertainty and $c\bar{c}$ correlations.** The direct and non-direct fractions for the charm background MC were varied in the same way as for beauty. The effect on the signal was small ($+0\%/-4\%$).
- **Trigger efficiency.** The uncertainty on the trigger efficiency was estimated by comparing the efficiencies for muon and non-muon triggers in data and MC ($\pm 5\%$).
- **Other uncertainties.** Other uncertainties include the variation of the like-/unlike-sign ratio for the false-muon background by 3% ($\pm 3\%$), the variation of the isolation cuts by up to 500 MeV ($\pm 2\%$), the variation of the E_T cut (energy scale) by 3% ($\pm 2\%$), the variation of the p_T^μ cuts (magnetic field uncertainty) by 0.3% ($< 1\%$).

The total systematic uncertainty (+25%/−28%) was obtained by adding the above contributions in quadrature. The uncertainties related to the background normalisation and the b and c spectral shape uncertainties were applied at a bin-by-bin level where relevant, while the others were added globally. A 2% overall normalisation uncertainty associated with the luminosity measurement was not included.

9 Total $b\bar{b}$ cross section

As a first step towards the extraction of the total cross section for $b\bar{b}$ production, a visible cross section was extracted for the maximum possible region in muon phase space allowed by the preselection and the detector acceptance (selection B). The criterion that the muon detection probability should be at least about 30% per muon leads to the following phase space definition at truth level:

- $-2.2 < \eta < 2.5$ for both muons;
- $p_T > 1.5$ GeV for one of the two muons;
- $p_T > 0.75$ GeV for the other muon, as well as $p > 1.8$ GeV for $\eta < 0.6$, or ($p > 2.5$ GeV or $p_T > 1.5$ GeV) for $\eta > 0.6$.

This cross-section definition refers to only one pair of muons per event. If there are more than two muons, muons directly originating from B hadron decays are taken preferentially to form the pair. A visible cross section for dimuon production from beauty decays in this phase space

$$\sigma_{\text{vis}}(ep \to b\bar{b}X \to \mu\mu X') = 55 \pm 7(\text{stat.})^{+14}_{-15}(\text{syst.})\ \text{pb} \tag{3}$$

was obtained. This cross section includes muons from direct B-hadron decays, and indirect decays via intermediate charm hadrons or τ leptons. The two muons can either originate from the same b quark, or from different quarks of the $b\bar{b}$ pair. Muonic decays of kaons, pions or other light hadrons were not included.

The measured cross section is larger than, but compatible with, the FMNR⊗Pythia NLO prediction

$$\sigma_{\text{vis,NLO}}(ep \to eb\bar{b}X \to e\mu\mu X) = 33^{+18}_{-8}(\text{NLO})^{+5}_{-3}(\text{frag.} \oplus \text{br.})\ \text{pb}, \tag{4}$$

where the first error refers to the uncertainties of the FMNR parton-level calculation, and the second error refers to the uncertainties related to fragmentation and decay.

The visible cross section was then translated into the total cross section for beauty production. The effective branching fraction of a $b\bar{b}$ pair into at least two muons is 6.3% [27, 43].

The probability (acceptance) for such a muon pair to be in the kinematic range of the measured visible cross section, evaluated from the beauty MC sample, is about 6% on average. Defining $p_{T,b}^{\max}$ as the maximum of the two b-quark transverse momenta after parton showering, and $|\zeta_b|^{\min}$ as the minimum of the modulus of the rapidity (not pseudo-rapidity) of the two quarks, this probability ranges from 3% for $p_{T,b}^{\max} = 0$ GeV to 9% at[6] $p_{T,b}^{\max} = 10$ GeV, for $|\zeta_b|^{\min} < 2$. The acceptance is almost independent of rapidity within this rapidity range, which covers 90% of the total $b\bar{b}$ phase space. It drops sharply at larger rapidities. Thus, only 10% of the total beauty contribution in the region $|\zeta_b|^{\min} > 2$ remains unmeasured. The small dependence of the acceptance on the transverse momenta of the b quarks is due to the low muon-momentum threshold, in combination with the large b-quark mass and the three-body decay kinematics. Sensitivity down to $p_T^b = 0$ GeV is obtained.

In summary, the combined probability for a $b\bar{b}$ pair to yield a muon pair in the visible kinematic range (6.3%×6%=0.38% on average) is quite small, but varies by less than a factor 3 over 90% of the total phase space. Furthermore, it is almost entirely determined by quantities measured [43] with good precision at e^+e^- colliders. These include the branching fractions listed in Table 1, the b-fragmentation functions, and the B hadron $\to \mu X$ decay spectra. It was checked that all of these are well reproduced by the MC after the application of branching-ratio corrections. The b-quark p_T and rapidity spectra predicted by the Pythia and Rapgap generators were found to agree with those from FMNR and HVQDIS to within 15% [29]. Furthermore, the quasi-uniformity of the acceptance explained above implies that the dependence on details of the simulation of the $b\bar{b}$ topology is rather weak. The MC can therefore safely be used for the extraction of the total cross section for beauty production.

The normalisation of the Pythia + Rapgap MC prediction for the beauty contribution had to be scaled up by a factor 1.84 to agree with the dimuon data. Applying this measured scale factor to the total Pythia and Rapgap cross sections, the total cross section for $b\bar{b}$ pair production in ep collisions at HERA for $\sqrt{s} = 318$ GeV was determined to be

$$\sigma_{\rm tot}(ep \to b\bar{b}X) = 13.9 \pm 1.5(\text{stat.})^{+4.0}_{-4.3}(\text{syst.})\ \text{nb}, \tag{5}$$

where the first uncertainty is statistical and the second systematic. In addition to the uncertainties described in Section 8, this includes an error of 5% from the uncertainties of the spectral shape mentioned above, and an error of 6% from the variation of the branching ratios, added in quadrature.

The total cross section predicted by next-to-leading-order QCD calculations was obtained in the massive approach by adding the predictions from FMNR [1] and HVQDIS [2] for

[6] At even larger p_T^b the acceptance rises further, but the fraction of events is small.

Q^2 less than or larger than 1 GeV^2, respectively. The resulting cross section for $\sqrt{s} = 318$ GeV

$$\sigma_{\rm tot}^{\rm NLO}(ep \to b\bar{b}X) = 7.5^{+4.5}_{-2.1}\ {\rm nb}$$

is a factor 1.8 lower than the measured value, although compatible within the large uncertainties. The corresponding cross section from FMNR only using the Weizsäcker-Williams approximation to estimate the DIS contribution is

$$\sigma_{\rm tot}^{\rm WW}(ep \to b\bar{b}X) = 7.8^{+4.9}_{-2.3}\ {\rm nb}, \tag{6}$$

in agreement with the more exact FMNR+HVQDIS calculation.

The fact that the comparisons between data and theory yield the same ratio at the visible level (Eqs. (3)/(4)):

$$R_{\rm vis}^{\rm data/NLO} = 1.7^{+0.7}_{-1.1}\ ;$$

and at quark level (Eqs. (5)/(6)):

$$R_{b}^{\rm data/NLO} = 1.8^{+0.8}_{-1.3}$$

confirms the validity of the extrapolation procedure used.

Figure 3 shows a comparison of the measured total cross section to cross sections and theoretical predictions from the $D^* + \mu$ final state obtained by ZEUS in earlier measurements [16]. Although not fully inclusive, these measurements are closest in phase space to the measurement presented here. Qualitatively, they show the same trend of the cross sections being higher than, but consistent with, the corresponding QCD predictions. The somewhat larger deviations reported in similar $D^* + \mu$ measurements by H1 [15] are not supported.

10 Differential cross sections and $b\bar{b}$ correlations

Selection A was used for the measurement of visible differential cross sections because a uniform kinematic acceptance is more relevant than maximal phase-space coverage. Correspondingly, at truth level, the phase space was restricted to:

- $p_T^\mu > 1.5$ GeV for both muons
- $-2.2 < \eta^\mu < 2.5$.

The backgrounds were again normalised as described in Section 7. The signal-extraction procedure was the same as for the inclusive visible cross section, except for being applied bin by bin. Bin-dependent systematic uncertainties were calculated wherever possible. The resulting cross sections for the differential p_T^μ and η^μ spectra are shown in Figs. 4

and 5. Very good agreement is observed with the PYTHIA+RAPGAP predictions scaled by the same factor 1.84 that was measured for the total cross section. Apart from the normalisation, the leading-order plus parton-shower (LO+PS) approach yields a good description of the corresponding physics processes within the entire accessible phase space. This confirms the applicability of these MC models for acceptance calculations.

A comparison of the measured cross sections to the absolute FMNR⊗PYTHIA NLO QCD predictions is also shown in Figs. 4 and 5. Again, good agreement in shape is observed, with a tendency to underestimate the data normalisation consistent with the observations from the total cross section. A potential trend for increasing data/theory deviations towards low p_T and/or high η, suggested by some previous measurements [10, 12], is not supported.

To provide a more detailed look at the correlations between the two b quarks, the reconstructed dimuon mass range was restricted[7] to $m^{\mu\mu} > 3.25$ GeV. This reduced the contribution of dimuons from the same quark to an almost negligible level. The corresponding data distribution for $\Delta\phi$ between the two muons is shown in Fig. 6. Figure 7 shows the resulting differential cross section, where the mass cut was replaced by the requirement that the two muons originate from different b quarks. The distribution is well described by the FMNR⊗PYTHIA NLO QCD predictions within the large uncertainties resulting from the subtraction method (Eq. (2)).

11 Hadron- and parton-level cross-sections

In order to compare to previous ZEUS results using other final states [11, 12], expressed in terms of parton-level cross sections[8] differential in p_T^b, similar cross sections were also extracted.

The first step was the extraction of visible cross sections for B hadrons in different p_T ranges. For this purpose, the data sample used for the measurement of the total beauty cross section (selection B) was split into two subsamples, with $m^{\mu\mu} > 3.25$ GeV and $m^{\mu\mu} < 3.25$ GeV. As motivated in the previous section, the $m^{\mu\mu} > 3.25$ sample is dominated by muons from different b quarks, with correlations between the two quarks which are reasonably understood. Thus, two measured B hadrons are present in each event. To estimate their transverse momenta, the quantitity

$$E_T^{\rm vis} = p_T^\mu + I^\mu$$

[7] While the mass separation value of 4 GeV described earlier was optimised such that all dimuons from the same b quark contribute to the low-mass sample, including dimuons from $b \to \psi\prime$ decays, the value 3.25 GeV was chosen to optimise the separation power for dimuons from same and different b quarks.

[8] H1 results have not been published in this form.

is evaluated for each muon, where I^μ is the cone transverse energy described in Section 4.4. This variable is found to be strongly correlated to the parent B hadron transverse momentum at high p_T, where the additional energy from b-quark fragmentation to the B hadron compensates the loss due to the unreconstructed neutrino from the semileptonic decay. At $p_T \lesssim m_b$, this correlation is diluted by the effect of the B-hadron mass and the corresponding decay kinematics. Figure 8(a) shows the expected B-hadron p_T spectra for three bins in $E_T^{\rm vis}$, $0 < E_T^{\rm vis} < 5$ GeV, $5 < E_T^{\rm vis} < 10$ GeV, and $10 < E_T^{\rm vis} < 40$ GeV. Reasonably distinct B-hadron p_T regions are probed. The corresponding visible cross sections are shown in Fig. 9(a).

A similar procedure was applied to the subsample with $m^{\mu\mu} < 3.25$ GeV. In this sample, the muons originate mainly from the same b quark, therefore only one B hadron has been measured. Due to branching ratios and decay kinematics, the cross section is smaller, but the absence of like-sign muon pairs from the same b quark leads to a smaller uncertainty from the subtraction method. Therefore, the precision of the measurement is comparable to that from the high-mass region. Furthermore, the subtraction method reduces the influence of the residual contribution of muons from different b quarks. Thus, the measured cross sections are almost completely insensitive to $b\bar{b}$ correlations.

The $E_T^{\rm vis}$ variable is redefined to

$$E_T^{\rm vis} = p_T^{\mu\mu} + I^\mu_{\rm high}$$

where $p_T^{\mu\mu}$ is the transverse momentum of the dimuon system added vectorially, and $I^\mu_{\rm high}$ is the isolation of the higher p_T muon only, to avoid double counting. The correlations to the B hadron p_T are similar to the high-mass case (Fig. 8(b)), enabling them to be combined later on. The resulting visible B-hadron cross sections are shown in Fig. 9(b).

For both subsamples, agreement is found with the FMNR⊗Pythia predictions, consistent with the conclusions obtained earlier.

The second step is to extrapolate these cross sections to b-quark level. For comparison with previous measurements, the cross sections were restricted to photoproduction. Each of the B-hadron visible cross sections is translated into a differential cross section $\frac{d\sigma}{dp_T^b}$ in the pseudorapidity range $|\eta_b| < 2$ [11] with photon virtuality $Q^2 < 1$ GeV^2 and inelasticity $0.2 < y < 0.8$, using the FMNR⊗Pythia predictions. Each cross section is quoted at the mean p_T^b value for events satisfying the cuts for the corresponding $E_T^{\rm vis}$ bin. The results are shown in Fig. 10.

The cross sections derived from the low- and high-mass subsamples (same and different b quarks) are in agreement, and were combined to give a single cross section for each p_T^b value. The maximum possible correlation of the systematic errors is assumed for this combination.

The resulting combined cross sections are compared to theory and previous measurements in Fig. 11. They are consistent with these previous measurements, and extend the measured range to lower p_T^b. Predictions at NLO [1] and predictions from a LO k_T-factorisation approach [34] yield an equally good description of the data.

12 Conclusions

The total cross section for beauty production in ep collisions at $\sqrt{s} = 318$ GeV has been measured for the first time using an analysis technique based on the detection of two muons, mainly from semileptonic beauty decay. The almost complete phase-space coverage combined with the weak dependence on details of the $b\bar{b}$ event topology allowed a reliable extraction of the total beauty production cross section, with acceptance down to $p_T^b = 0$ GeV, and a direct comparison to NLO QCD predictions. The predictions are lower than the observed cross sections, but compatible within the uncertainties. Differential cross sections in p_T^μ, η^μ, and $\Delta\phi^{\mu\mu}$ were also measured. Shapes predicted by Monte Carlo models incorporating leading-order matrix elements followed by parton showers agree well with the data. NLO QCD predictions agree in shape with both the data and the LO+PS predictions, but are again somewhat lower than the data, in agreement with the observation from the total cross section. The angular correlations between final-state muons from different b quarks, reflecting the correlations between these parent quarks, are described by the NLO QCD predictions. Measurements of cross sections for muon pairs from the same or from different B hadrons yield similar and compatible results. A comparison with previous measurements through the extrapolation to differential cross sections at b-quark level shows reasonable agreement, and extends these measurements down to lower p_T^b.

Acknowledgements

We thank the DESY Directorate for their strong support and encouragement. The remarkable achievements of the HERA machine group were essential for the successful completion of this work and are greatly appreciated. We are grateful for the support of the DESY computing and network services. The design, construction and installation of the ZEUS detector have been made possible owing to the ingenuity and effort of many people who are not listed as authors. It is also a pleasure to thank S. Frixione for help with the theoretical predictions.

References

[1] S. Frixione et al., Nucl. Phys. **B 412**, 225 (1994);
S. Frixione, P. Nason and G. Ridolfi, Nucl. Phys. **B 454** (1995);
M. Cacciari, S. Frixione and P. Nason, JHEP **0103**, 006 (2001).

[2] B.W. Harris and J. Smith, Nucl. Phys. **B 452**, 109 (1995);
B.W. Harris and J. Smith, Phys. Lett. **B 353**, 535 (1995). Erratum-ibid **B 359** (1995) 423;
B.W. Harris and J. Smith, Phys. Rev. **D 57**, 2806 (1998).

[3] UA1 Coll., C. Albajar et al., Phys. Lett. **B 186**, 237 (1987);
UA1 Coll., C. Albajar et al., Phys. Lett. **B 213**, 405 (1988);
UA1 Coll., C. Albajar et al., Phys. Lett. **B 256**, 121 (1991). Erratum-ibid. **B 262**, 497 (1991);
UA1 Coll., C. Albajar et al., Z. Phys. **C 61**, 41 (1994).

[4] CDF Coll., F. Abe et al., Phys. Rev. Lett. **71**, 500 (1993);
CDF Coll., F. Abe et al., Phys. Rev. Lett. **71**, 2396 (1993);
CDF Coll., F. Abe et al., Phys. Rev. Lett. **75**, 1451 (1995);
CDF Coll., F. Abe et al., Phys. Rev. **D 53**, 1051 (1996);
CDF Coll., F. Abe et al., Phys. Rev. **D 55**, 2546 (1997);
CDF Coll., D. Acosta et al., Phys. Rev. **D 65**, 052005 (2002);
CDF Coll., D. Acosta et al., Phys. Rev. **D 66**, 032002 (2002);
CDF Coll., D. Acosta et al., Phys. Rev. **D 71**, 032001 (2005);
CDF Coll., D. Acosta et al., Phys. Rev. **D 71**, 092001 (2005);
CDF Coll., T. Aaltonen et al., Preprint arXiv:0710.1895 [hep-ex], 2007;
DØ Coll., S. Abachi et al., Phys. Rev. Lett. **74**, 3548 (1995);
DØ Coll., B. Abbott et al., Phys. Lett. **B 487**, 264 (2000);
DØ Coll., B. Abbott et al., Phys. Rev. Lett. **84**, 5478 (2000);
DØ Coll., B. Abbott et al., Phys. Rev. Lett. **85**, 5068 (2000).

[5] L3 Coll., M. Acciarri et al., Phys. Lett. **B 503**, 10 (2001);
L3 Coll., P. Achard et al., Phys. Lett. **B 619**, 71 (2005).

[6] ALEPH Coll., S. Schael et al., JHEP **0709**, 102 (2007).

[7] WA78 Coll., M. Catanesi et al., Phys. Lett. **B 202**, 453 (1988);
E672/E706 Coll., R. Jesik et al., Phys. Rev. Lett. **74**, 495 (1995).

[8] E771 Coll., T. Alexopoulos et al., Phys. Rev. Lett. **82**, 41 (1999);
D.M. Jansen et al., Phys. Rev. Lett. **74**, 3118 (1995);
HERA–B Coll., I. Abt et al., Eur. Phys. J. **C 26**, 345 (2003).

[9] H1 Coll., C. Adloff et al., Phys. Lett. **B 467**, 156 (1999);
ZEUS Coll., J. Breitweg et al., Eur. Phys. J. **C 18**, 625 (2001).

[10] H1 Coll., A. Aktas et al., Eur. Phys. J. **C 41**, 453 (2005).

[11] ZEUS Coll., S. Chekanov et al., Phys. Rev. **D 70**, 12008 (2004). Erratum-ibid **D 74**, 059906 (2006).

[12] ZEUS Coll., S. Chekanov et al., Phys. Lett. **B 599**, 173 (2004).

[13] ZEUS Coll., S. Chekanov et al., Preprint DESY-08-056, 2008.

[14] H1 Coll., A. Aktas et al., Eur. Phys. J. **C 40**, 349 (2005);
H1 Coll., A. Aktas et al., Eur. Phys. J. **C 45**, 23 (2006);
H1 Coll., A. Aktas et al., Eur. Phys. J. **C 47**, 597 (2006).

[15] H1 Coll., A. Aktas et al., Phys. Lett. **B 621**, 56 (2005).

[16] ZEUS Coll., S. Chekanov et al., Eur. Phys. J. **C 50**, 1434 (2007).

[17] ZEUS Coll., U. Holm (ed.), *The ZEUS Detector*. Status Report (unpublished), DESY (1993), available on `http://www-zeus.desy.de/bluebook/bluebook.html`.

[18] N. Harnew et al., Nucl. Inst. Meth. **A 279**, 290 (1989);
B. Foster et al., Nucl. Phys. Proc. Suppl. **B 32**, 181 (1993);
B. Foster et al., Nucl. Inst. Meth. **A 338**, 254 (1994).

[19] M. Derrick et al., Nucl. Inst. Meth. **A 309**, 77 (1991);
A. Andresen et al., Nucl. Inst. Meth. **A 309**, 101 (1991);
A. Caldwell et al., Nucl. Inst. Meth. **A 321**, 356 (1992);
A. Bernstein et al., Nucl. Inst. Meth. **A 336**, 23 (1993).

[20] G. Abbiendi et al., Nucl. Instr. and Meth. **A 333**, 342 (1993).

[21] P. Plucinski, Ph.D. Thesis, Institute for Nuclear Studies, Warsaw (Poland), 2008.

[22] I. Bloch, Ph.D. Thesis, Hamburg University, Hamburg (Germany), Report DESY-THESIS-2005-034, DESY, 2005.

[23] W.H. Smith, K. Tokushuku and L.W. Wiggers, *Proc. Computing in High-Energy Physics (CHEP), Annecy, France, Sept. 1992*, C. Verkerk and W. Wojcik (eds.), p. 222. CERN, Geneva, Switzerland (1992). Also in preprint DESY 92-150B.

[24] ZEUS Coll., S. Chekanov et al., Nucl. Phys. **B 729**, 492 (2005).

[25] ZEUS Coll., S. Chekanov et al., Eur. Phys. J. **C 44**, 13 (2005).

[26] G.M. Briskin, Ph.D. Thesis, Tel Aviv University, Report DESY-THESIS 1998-036, 1998.

[27] T. Sjöstrand, Comp. Phys. Comm. **82**, 74 (1994).

[28] H. Jung, Comp. Phys. Comm. **86**, 147 (1995).

[29] A. Longhin, Ph.D. Thesis, Università di Padova, Padova (Italy), Report DESY-THESIS-2004-050, Università di Padova and INFN, 2004.

[30] G. Marchesini et al., Comp. Phys. Comm. **67**, 465 (1992).

[31] T. Abe, Comput. Phys. Commun. **136**, 126 (2001).

[32] R. Brun et al., GEANT3, Technical Report CERN-DD/EE/84-1, CERN, 1987.

[33] J. Binnewies, B.A. Kniehl and G. Kramer, Z. Phys. **C 76**, 677 (1997);
B.A. Kniehl, G. Kramer and M. Spira, Z. Phys. **C 76**, 689 (1997);
J. Binnewies, B.A. Kniehl and G. Kramer, Phys. Rev. **D 48**, 014014 (1998).

[34] A. Lipatov and N. Zotov, Phys. Rev. **D 73**, 114018 (2006);
A. Lipatov and N. Zotov, JHEP **0608**, 043 (2006);
H. Jung, Phys. Rev. **D 65**, 034015 (2002);
H. Jung, J. Phys. **G 28**, 971 (2002).

[35] C.F. von Weizsäcker, Z. Phys. **88**, 612 (1934);
E.J. Williams, Phys. Rev. **45**, 729 (1934);
S. Frixione et al., Phys. Lett. **B 319**, 339 (1993).

[36] CTEQ Coll., H.L. Lai et al., Eur. Phys. J. **C 12**, 375 (2000).

[37] M. Glück, E. Reya, and A. Vogt, Phys. Rev. **D 46**, 1973 (1992).

[38] See e.g. CDF Coll., A. Abulencia et al., Phys. Rev. **D 75**, 092006 (2007). Erratum-ibid. **D 75** 119901, 2007.

[39] ZEUS Coll., S. Chekanov et al., Eur. Phys. J. **C 44**, 183 (2005).

[40] A. Geiser, *Proc. 5th International Workshop on Deep-Inelastic Scattering and Related Subjects (DIS2007)*, Munich, Germany, 16-20 Apr 2007, G. Grindhammer and K. Sachs (eds.), Vol 2, p. 883. DESY, Hamburg, Germany (2008), doi:10.3360/dis.2007.163. Also in preprint arXiv:0711.1983 [hep-ex], 2007.

[41] A. Geiser and A.E. Nuncio-Quiroz, J. Phys. Conf. Ser. **110**, 022036 (2008);
A.E. Nuncio-Quiroz, Ph.D. Thesis, Hamburg University, Hamburg (Germany), Report to be published as DESY-THESIS, DESY, 2008.

[42] S. Frixione and B.R. Webber, JHEP **06**, 029 (2002);
S. Frixione, P. Nason and B.R. Webber, JHEP **08**, 007 (2003).

[43] Particle Data Group, W.-M. Yao et al., J. Phys. **G 33**, 1 (2006).

[44] U. Samson, Ph.D. Thesis, Bonn University, Bonn (Germany), Report Bonn-IR-2008-06, 2008.

channel	effective branching fraction w/o $B^0\bar{B}^0$ mixing
$b \to \mu^-$ direct	10.95 ± 0.27 %
$b \to \mu^+$ indirect	8.27 ± 0.40 %
$b \to \mu^-$ indirect	2.21 ± 0.50 %
all $b \to \mu^\pm$	21.43 ± 0.70 %
$b\bar{b} \to \mu^\pm\mu^\mp$ (diff. bs)	2.42 ± 0.17 %
$b\bar{b} \to \mu^\pm\mu^\pm$ (diff. bs)	2.18 ± 0.14 %
$b \to \mu^+\mu^-$ all	2.40 ± 0.16 %

Table 1: *Effective branching fractions used for cross-section determinations. The indirect contributions include cascade decays into muons via charm, anticharm, $\tau^\pm$ and J/ψ. The additional effect of $B^0\bar{B}^0$ mixing ($\chi = 0.1283 \pm 0.0076$) is not included.*

	unlike-sign $\pm/\mp$	like-sign $++$ / $--$
low inv. mass $m_{\mu\mu} < 4$ GeV	**muons from same b**, muons from J/ψ, ψ', and false-muon background	**false-muon background**, and small contribution of muons from different b
high inv. mass $m_{\mu\mu} > 4$ GeV	**muons from different b**, muons from $c\bar{c}$, Υ, BH, and false-muon background	**muons from different b** and false-muon background

Table 2: *Classification of events using dimuon mass and charge correlations. The main contributions to each class are listed; the most relevant is indicated in bold face.*

process	muon candidates
beauty	2382
charm	629
quarkonia and BH	281
false muon	1281
data	4574

Table 3: *Number of muon candidates contributing to Fig. 2: unlike-sign non-isolated dimuons. 4574 muons correspond to 2287 events.*

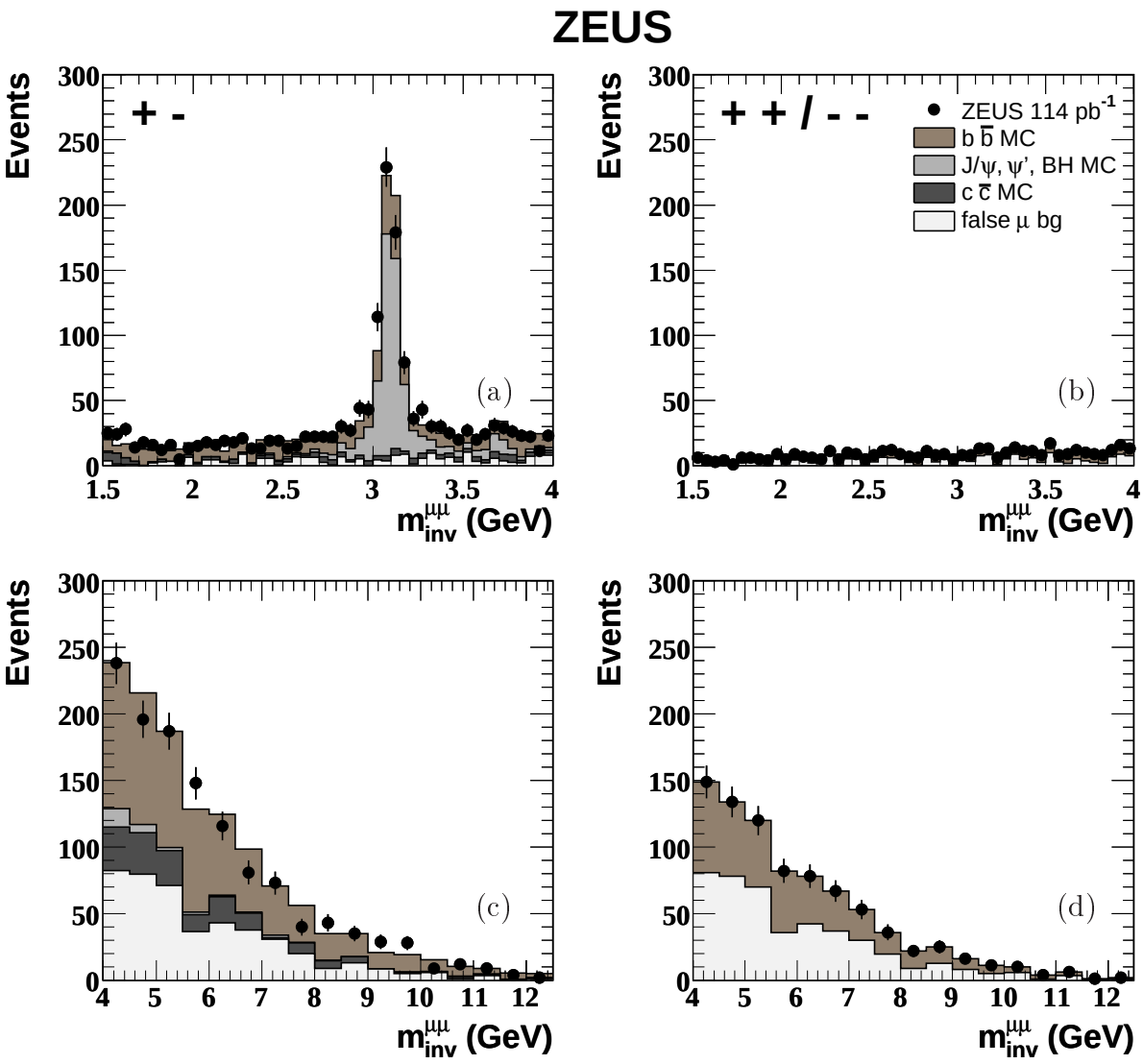

Figure 1: *Dimuon mass distributions of unlike-sign dimuon pairs from selection B (see text) in the (a) low-mass and (c) high-mass subsamples, as well as like-sign dimuon pairs in the (b) low-mass and (d) high-mass subsamples. The same vertical scale has been chosen for the like- and unlike-sign subsamples, with different bin sizes for the high- and low-mass regions. The expected contributions from different processes are also shown. The false-muon background was obtained from the data using the subtraction method described in Section 3. Due to this method, the total prediction for like-sign pairs agrees with the data by definition.*

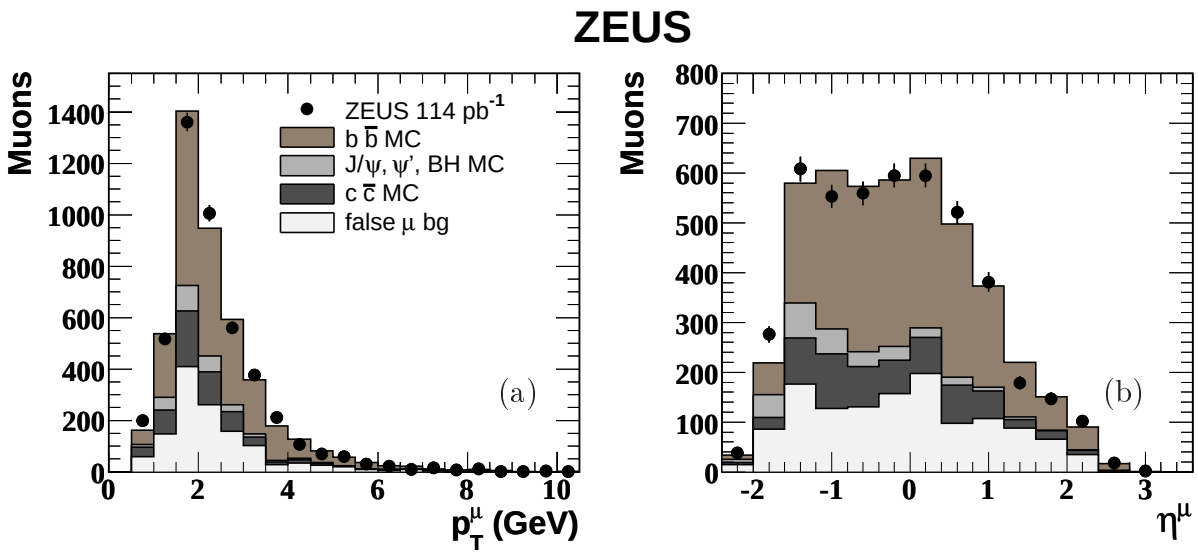

Figure 2: *(a) Muon transverse momentum and (b) muon pseudorapidity distribution from both high- and low-mass dimuon pairs in the non-isolated unlike-sign sample. Two muons are entered for each event. The expected contributions from different processes are also shown. Due to the subtraction method, the statistical error of the prediction for the false-muon background is comparable in absolute size to that of the data.*

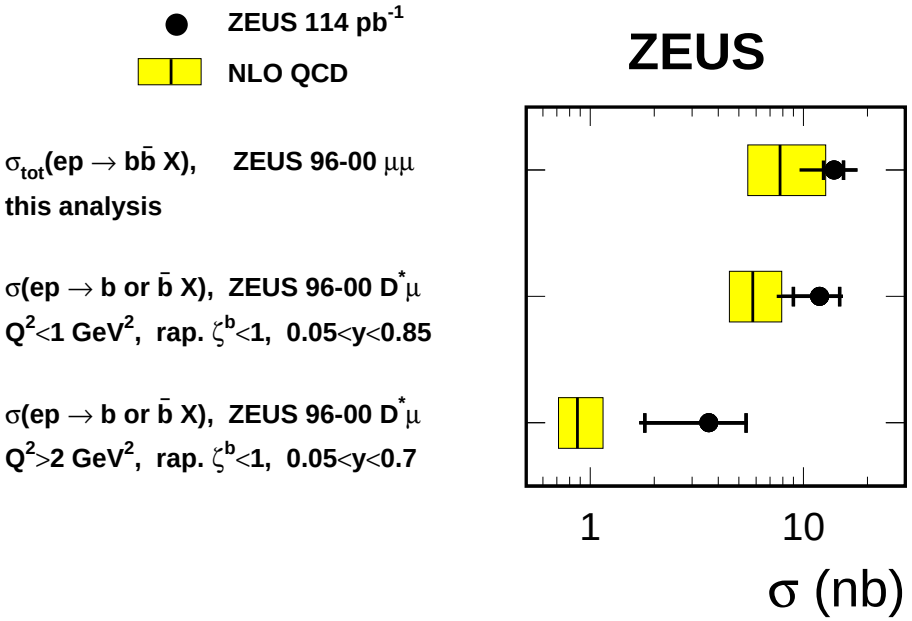

Figure 3: *Comparison of measured cross sections to NLO QCD predictions. The $b\bar{b}$ cross section from this analysis (top) is compared to both measured and predicted b or $\bar{b}$ cross sections obtained in the ZEUS $D^*\mu$ analysis [16] for the photoproduction regime (middle line) and DIS (lower line). The NLO calculations in the $D^*\mu$ analysis used a slightly different set of parameters. Using the parameters detailed in Section 6, the central value of the photoproduction cross-section prediction would increase by about 20%.*

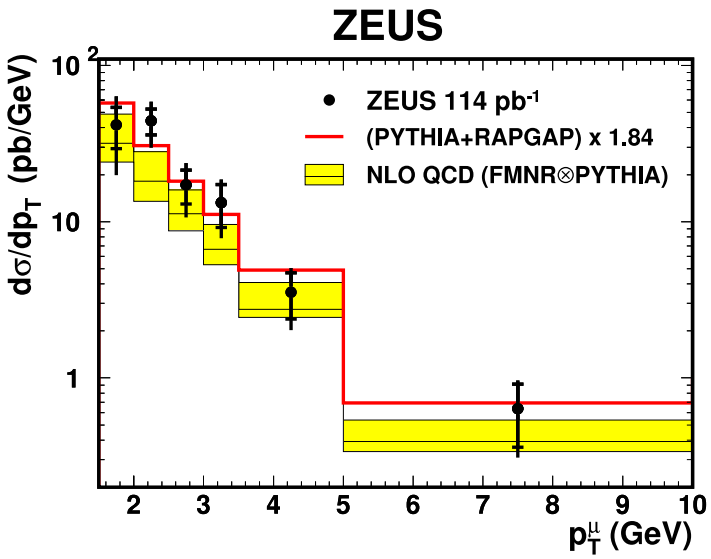

Figure 4: *Cross-section $d\sigma/dp_T^\mu$ for muons from b decays in dimuon events with $p_T^\mu > 1.5$ GeV and $-2.2 < \eta^\mu < 2.5$ for both muons. Two muons contribute for each event. The data (solid dots) are compared to the scaled sum of the predictions by the LO+PS generators* PYTHIA *and* RAPGAP *(histogram) and to the NLO QCD predictions from* FMNR⊗PYTHIA *(band).*

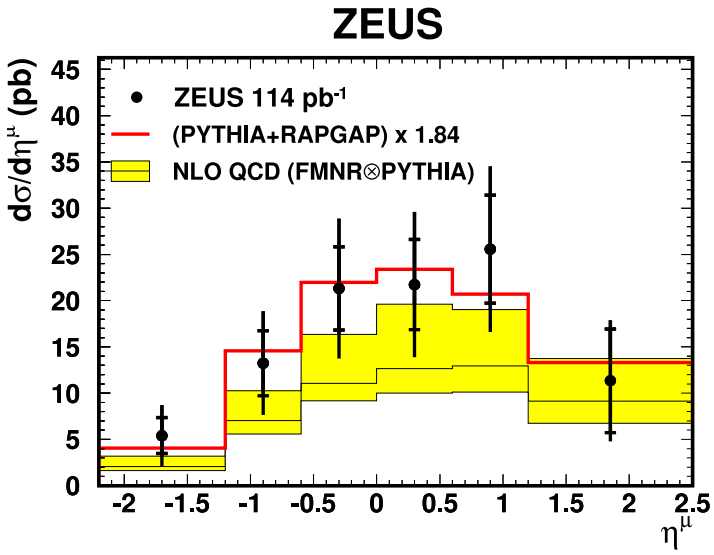

Figure 5: *Cross-section $d\sigma/d\eta^\mu$ for muons from b decays in dimuon events with $p_T^\mu > 1.5$ GeV and $-2.2 < \eta^\mu < 2.5$ for both muons. Two muons contribute for each event. The data (solid dots) are compared to the scaled sum of the predictions by the LO+PS generators* PYTHIA *and* RAPGAP *(histogram) and to the NLO QCD predictions from* FMNR⊗PYTHIA *(band).*

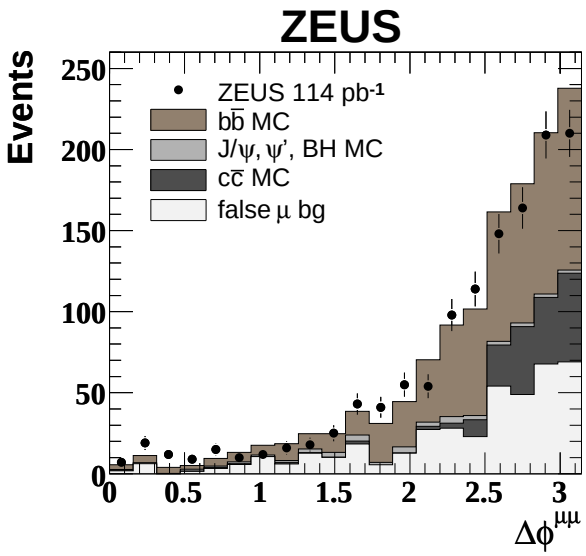

Figure 6: *Distribution of the azimuthal distance $\Delta\phi$ between the two muons in dimuon events with $p_T^\mu > 1.5$ GeV for both muons, and $m^{\mu\mu} > 3.25$ GeV. The expected contributions from different processes are also shown. Due to the subtraction method, the statistical error of the prediction for the false muon background is comparable in absolute size to that of the data.*

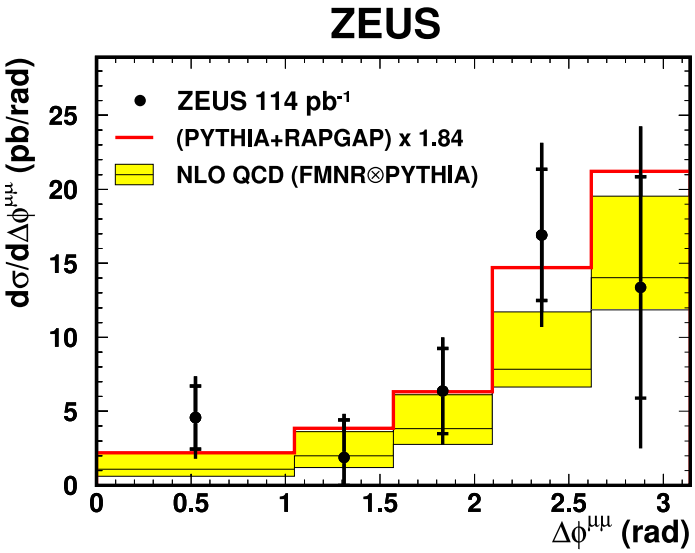

Figure 7: *Cross-section $d\sigma/d\Delta\phi^{\mu\mu}$ for $b\bar{b}$ events in which the muons originate from different b quarks, with $p_T^\mu > 1.5$ GeV and $-2.2 < \eta^\mu < 2.5$ for both muons. The data (solid dots) are compared to the scaled sum of the predictions by the LO+PS generators* Pythia *and* Rapgap *(histogram) and to the NLO QCD predictions from* FMNR⊗Pythia *(band).*

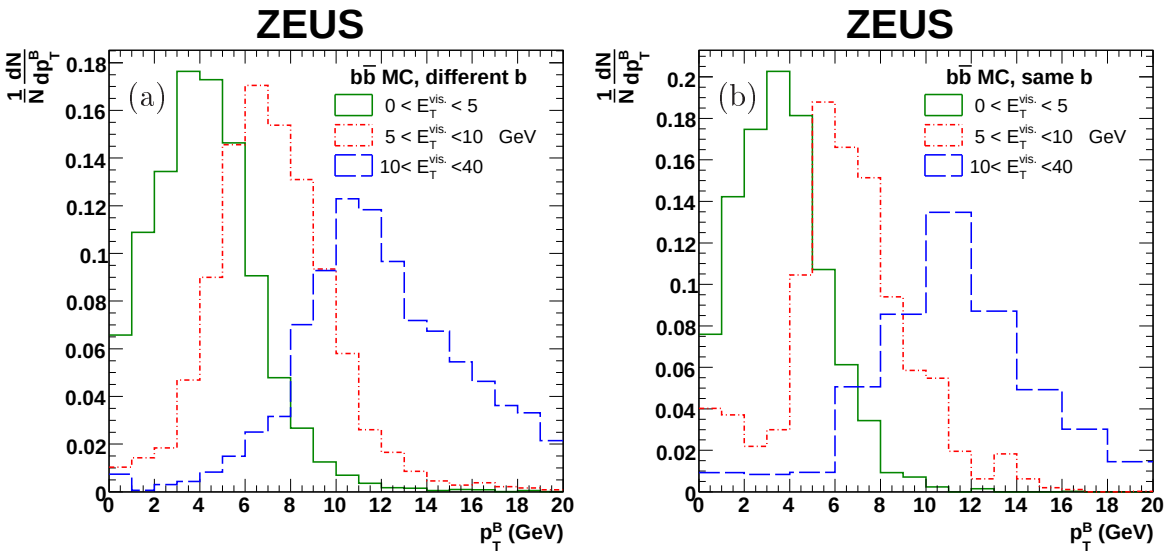

Figure 8: *Distribution of the true p_T of the parent B hadron for muons from (a) different b quarks or from (b) the same b quark, for the three E_T^{vis} bins indicated in the figures. For the definition of E_T^{vis}, see Section 11.*

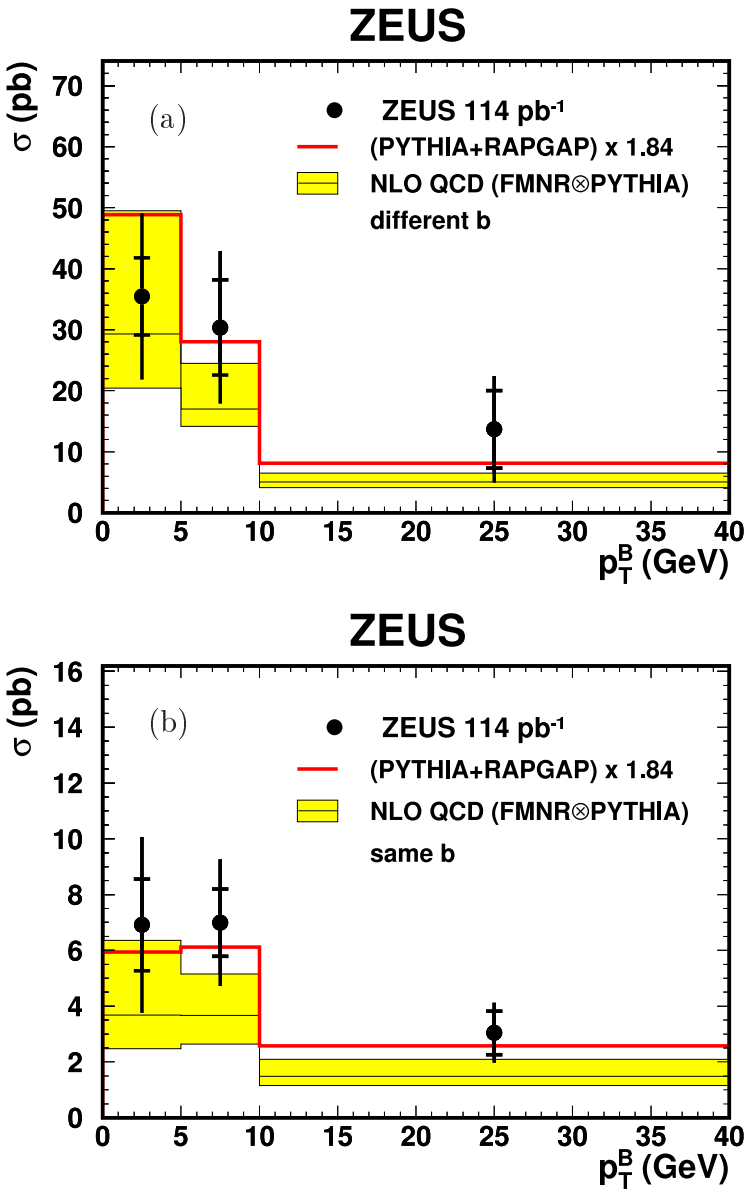

Figure 9: *Visible cross section for parent B hadrons from events containing two muons satisfying the cuts for the total cross-section measurement, and in which both muons originate from a different (a) or from the same $b(\bar{b})$ quark (b), in three bins of p_T^B. There are two entries per event for (a), and one entry per event for (b). The data (solid dots) are compared to the scaled sum of the predictions by the LO+PS generators* Pythia *and* Rapgap *(histogram) and to the NLO QCD predictions from* FMNR⊗Pythia *(band).*

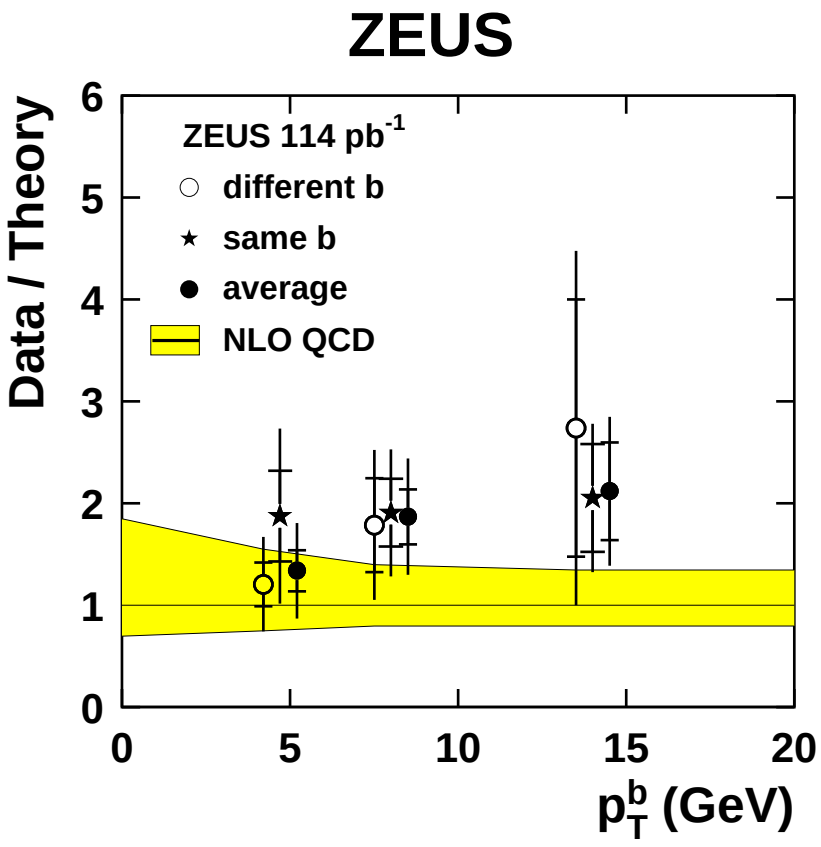

Figure 10: *Data/NLO ratio for cross sections from different b quarks (open circles) compared to measurements from the same b quark (stars) and their average (filled circles). The value for each E_T^{vis} (or p_T^B) interval (0-5,5-10,10-40 GeV) is quoted at the median p_T of the parent b quarks in events satisfying all detector level cuts (4.7,8.0,14.0 GeV). The three points for each p_T^b value are shown slightly shifted in p_T^b for clarity.*

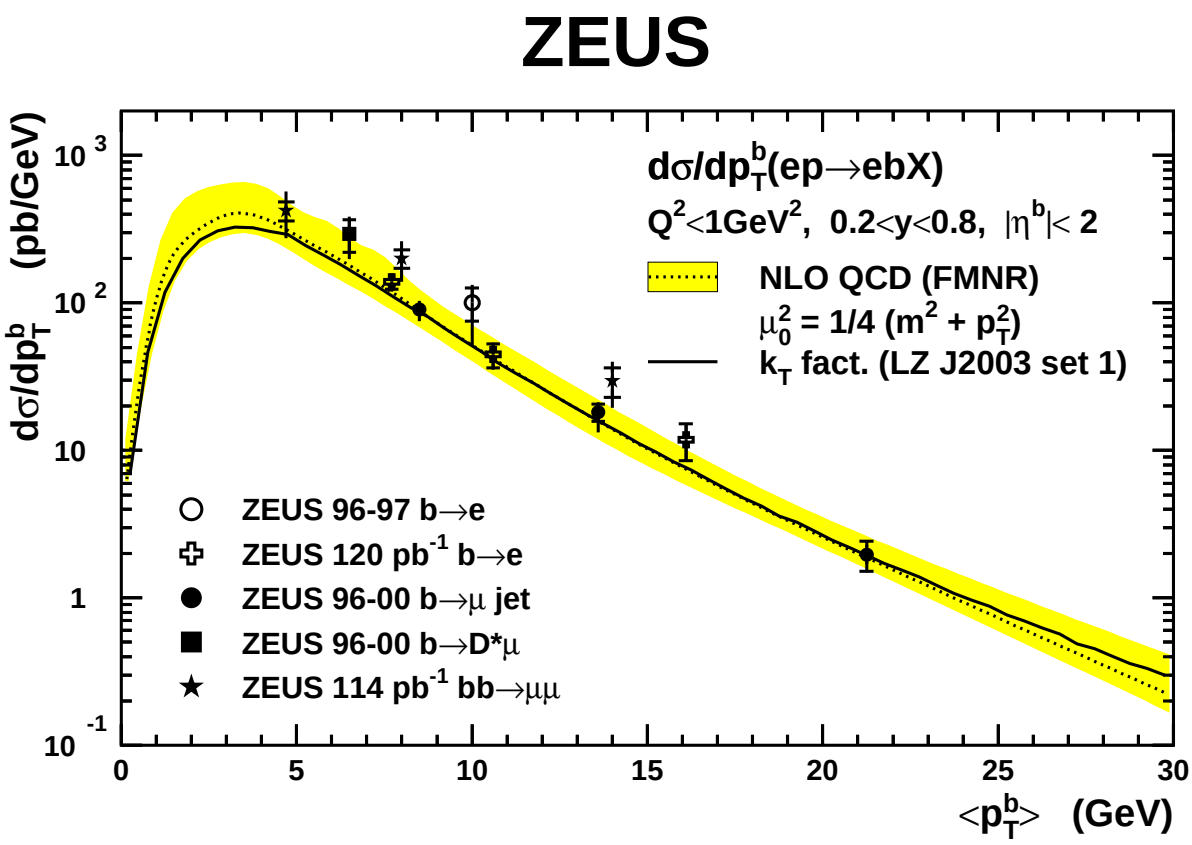

Figure 11: *Differential cross section $d\sigma/dp_T^b$ of this analysis (stars) compared to previous ZEUS measurements (other symbols), FMNR NLO QCD predictions (band), and predictions from the k_T factorisation approach (thick line).*